

Article

Impacts on Noise Analyses of GNSS Position Time Series Caused by Seasonal Signal, Weight Matrix, Offset, and Helmert Transformation Parameters

Guo Chen ^{1,2} , Qile Zhao ^{2,3}, Na Wei ^{2,*}  and Jingnan Liu ^{2,3,*}

¹ School of Geodesy and Geomatics, Wuhan University, No. 129 Luoyu Road, Wuhan 430079, China; guo_chen@whu.edu.cn

² GNSS Research Center, Wuhan University, No. 129 Luoyu Road, Wuhan 430079, China; zhaoql@whu.edu.cn

³ Collaborative Innovation Center of Geospatial Technology, Wuhan University, No. 129 Luoyu Road, Wuhan 430079, China

* Correspondence: nwei@whu.edu.cn (N.W.); jnliu@whu.edu.cn (J.L.)

Received: 6 September 2018; Accepted: 30 September 2018; Published: 2 October 2018



Abstract: The noise characteristics of the Global Navigation Satellite System (GNSS) position time series can be biased by many factors, which in turn affect the estimates of parameters in the deterministic model using a least squares method. The authors assess the effects of seasonal signals, weight matrix, intermittent offsets, and Helmert transformation parameters on the noise analyses. Different solutions are obtained using the simulated and real position time series of 647 global stations and power law noise derived from the residuals of stacking solutions are compared. Since the true noise in the position time series is not available except for the simulated data, the authors paid most attention to the noise difference caused by the variable factors. First, parameterization of seasonal signals in the time series can reduce the colored noise and cause the spectral indexes to be closer to zero (much “whiter”). Meanwhile, the additional offset parameters can also change the colored noise to be much “whiter” and more offsets parameters in the deterministic model leading to spectral indexes closer to zero. Second, the weight matrices derived from the covariance information can induce more colored noise than the unit weight matrix for both real and simulated data, and larger biases of annual amplitude of simulated data are attributed to the covariance information. Third, the Helmert transformation parameters (three translation, three rotation, and one scale) considered in the model show the largest impacts on the power law noise (medians of $0.4 \text{ mm}^{-k/4}$ and 0.06 for the amplitude and spectral index, respectively). Finally, the transformation parameters and full-weight matrix used together in the stacking model can induce different patterns for the horizontal and vertical components, respectively, which are related to different dominant factors.

Keywords: seasonal signal; weight matrix; offset; transformation parameters; noise analyses

1. Introduction

Global Navigation Satellite System (GNSS) techniques play an important role in the discovery and validation of Earth geodynamic phenomena. Using the GNSS position time series of stations distributed in global or regional networks, many studies were carried out in wide fields, such as tectonic motion, sea level uplift, co-seismic and post-seismic deformations, postglacial rebound, Earth surface mass redistribution, and so on. It is well known that the deterministic function model and stochastic model jointly affect the interpretation and conclusion of the same geodynamic phenomenon based on the parameters estimates and uncertainty derived from the post-processing of GNSS precise positioning [1,2].

In order to obtain reliable estimates of station velocity, it is crucial to model the characteristics of stochastic processes in the GNSS position time series [3]. With the contributions of many researchers, it has been generally accepted that the error in the position time series cannot be described by purely white noise. Langbein and Johnson analyzed the two-color electronic distance measurements in California and demonstrated that power law noise dominates at lower frequencies in the geodetic time series [4]. Zhang et al. estimated the slope of power spectra of the daily position time series of 10 continuously monitoring Global Positioning System (GPS) sites in southern California with a 19-month time span, and suggested that fractal white noise processes (i.e., power law noise) with spectral indexes around 0.4 are suitable for the stochastic errors [5]. Wang et al. studied the noise properties of continuous GPS time series for the Crustal Movement Observation Network of China (CMONOC) and demonstrated that the white-plus-flicker noise model is preferred for 98.7% of stations with the unfiltered solutions. Without a common mode error, about 74% of the position time series are characterized by white-plus-flicker noise and the rest by the combination of white noise and a random walk noise model [6]. The colored noise influences the error properties in the position time series of stations from both regional networks and global network. Mao et al. assessed the noise characteristics of the daily GPS position series of 23 global stations [7]. The results from both power spectral analyses (PSA) and maximum likelihood estimation (MLE) indicated that a combination of a white and flicker noise models was able to best describe the noise characteristics of all three components. Using the homogeneously reprocessed solutions of 275 globally distributed stations, Santamaría-Gómez et al. found that the best noise model describing the correlated errors in the position time series was a combination of variable white noise and power law noise models [8]. Williams et al. confirmed the colored noise exists both in the position time series of global and regional solutions, and the white noise plus flicker noise is clearly the dominant noise model. Meanwhile, they demonstrated that the white and flicker noise amplitudes show latitude dependence [9].

The presence of temporally-correlated stochastic error (i.e., colored noise) in the noise analyses can be caused by many factors. In order to avoid the misinterpretation of time correlation noise caused by unmodeled periodic signals in position time series, Amiri-Simkooei adopted the least squares harmonic estimation (LS-HE) method to capture the periodic signals and took the significant periodic signals as the deterministic part in the functional model [10]. Bogusz and Klos indicated that the amplitudes of power law noise decrease and the spectral indexes are closer to zero when all periodicities from the first to ninth harmonics of the residual Chandler, tropical, and GPS draconitic were considered in the deterministic model compared to the traditional function model [11]. Moreover, the unmodeled bedrock thermal and environmental loading deformation, or inadequacies in the models of solar radiation pressure, mapping functions, and a priori zenith hydrostatic delays could introduce significant periodic signals and time-correlated noise in the position time series [12–14].

Williams pointed out that the undetected offsets could mimic random walk noise and the effect of offsets estimation in the position time series on velocity uncertainty depends on the noise properties [15]. The presence of unmodeled transient events (e.g., post-seismic deformation and slow slip events) will exhibit a significant component of time correlated noise, and the noise can be reduced after subtracting the transient deformations from the time series [16]. Liao et al. validated that the spectral indexes of the power law noise before and after the 2008 Wenchuan M8.0 earthquake have significant differences, which demonstrated that processing the data of the pre- and post-seismic together is not acceptable [17].

Santamaría-Gómez et al. tested some sources of the time-correlated noise and indicated that the amplitude of temporal noise depends on the data period rather than the increasing ambiguity fixed rate or the increasing number of observed satellites [8]. The improved temporal stability of receivers and satellites contributes to the noise evolution. Moreover, monument noise in the GNSS position time series is always believed to be a random walk process and the deep-drilled braced monument seems to have the least amplitude of random walk noise [9]. Jiang et al. indicated that, with the higher-order

ionospheric (HOI) correction considered, white noise amplitude in the up direction decreased by 81.8%, while flicker noise amplitudes in the north direction decreased by 67.5% [18].

Using the same data source, the authors assessed the effects of the Helmert transformation parameters and weight matrix on the seasonal signals in the GNSS position time series, and the contribution of environmental loading displacements to the seasonal signals was also assessed [19]. It is well known that the combination of deterministic and stochastic models jointly dominates the estimates. The authors are to assess the impacts of the seasonal signal and weight matrix, as well as the offset and Helmert transformation parameters on noise properties in the GNSS position time series. The noise analysis results may be used to refine the a priori stochastic model for the parameters adjustment. Many researchers focus on the noise characteristics of time series, but the possible systematic errors for the estimation of colored noise properties caused by the above factors are neglected.

Previous studies focused on the noise analyses for position time series in each direction and the spatial correlations between any two stations in the regional or global network were neglected when generating a cumulative solution. In this study, to investigate the effect of the spatial correlations on the noise analyses and parameters estimation in the deterministic model, the full covariance information representing the correlations between different stations, are taken into account. During the analyses of colored noise, the annual and semiannual signals in the position time series were always modeled. However, the results of mutual effects between the seasonal signals and the noise analyses results were not available. Moreover, most studies focused on the effects on the velocity bias and uncertainty of offsets in the position time series [15,20,21]. The authors in this study provide a different view by assessing the effect of offsets on colored noise; meanwhile, the mutual impacts on each other between seasonal signals and noise process are also demonstrated. Previous studies always aligned the precise coordinates of stations to the International Terrestrial Reference Frame (ITRF) using similarity transformation method before noise analyses [6,17,22], and no transformation parameters are considered in the stacking of position time series. It is unclear to what extent the transformation parameters (three translation, three rotation, and one scale parameters) affected noise analyses.

In order to assess the effects of the weight matrix, seasonal signals, offsets, and transformation parameters on the noise analyses results, this study is organized as follows. The practical position the data source is introduced and collected in Section 2. Afterward, the processing strategies of the position time series are described, and simulated data are also generated in this section for further analyses. Based on the simulated and real GNSS position time series, the results of colored noise analyses in GNSS position time series are demonstrated in Section 3 and discussed in Section 4. Finally, the study is concluded in Section 5.

2. Materials and Methods

2.1. Data Collection

Since the official service started on 1 January 1994, the International GNSS Service (IGS) has been supporting studies into the Earth sciences and fundamental astronomy. Thanks to the contribution of global analysis centers and the success of the experimental satellite orbit combination in 1993, IGS now provides users kinds of high-quality, official combined products, which include tracking station coordinates and clock biases, Earth rotation parameters (ERP), GPS satellite orbit and clock biases, and global ionosphere maps [23,24].

Thanks to the refinement and optimization of models and methodology in GNSS data processing over time, the quality of IGS solutions have achieved continuous improvements. It is also necessary to reanalyze the historical GNSS data collected from the IGS global network in a fully consistent way with the latest models and methodology. Until now, the IGS has completed two reprocessing campaigns, and the second one was finalized in 2015. Compared with the first one, there are some main characteristics in the second reprocessing, including a switch from weekly to daily solutions, a modification for the yaw-attitude models for the GPS Block IIA/IIR and GLONASS-M satellites [25,26], the Earth

radiation pressure considered in the dynamic model [27], and the implementation of International Earth Rotation Service (IERS) 2010 Conventions and IGB08/igs.08.atx reference frame [28]. More details about the IGS second data reprocessing campaign can be found at the website of IGS (<http://acc.igs.org/reprocess2.html>).

Compared with the solution from the individual analysis center (AC), the combination of multi-analysis centers (ACs) is thought to be more reliable than, and at least as accurate as, the solution obtained from each AC. Moreover, the combined solutions with more stations than any individual AC are generated. In this study, the combined IGS second reprocessed daily solutions are collected during the time from January 1994 to February 2015. The coordinates of stations, Earth rotation parameter (ERP), and apparent geocenter motion parameter (GCMP) are processed simultaneously to obtain consistent combined solutions. Adopting the constraints of no-net-rotation (NNR) and no-net-translation (NNT) on the selected core stations, the daily combined solutions are aligned to the IGB08 reference frame [29]. From the comparison between the solutions of ACs and the combinations, the inter-AC agreement is 1.5 mm and 4 mm for the horizontal and vertical components of stations coordinates, respectively. Regarding the ERPs, the agreement of 25–40 μs for pole coordinates, 140–40 $\mu\text{s}/\text{day}$ for the pole rate, and 8–20 $\mu\text{s}/\text{day}$ for the calibrated length of day estimates were obtained [29]. All the adjusted parameters and their corresponding variance information are stored in the daily files with the form of solution independent exchange (SINEX). With all this a priori and post information, the normal equation could be recovered and used for further processing.

2.2. GNSS Position Time Series Processing Strategies

The daily combined solutions from the IGS were used to stack for a cumulative solution in this study. The stacking model was similar to the Equation (1) of Reference [19], but an additional scale parameter was considered for some tests in this study.

$$\mathbf{x}_i^s(t_k) + \mathbf{v}_i^s(t_k) = \mathbf{x}_i^c(t_0) + \dot{\mathbf{x}}_i^c(t_k - t_0) + \mathbf{T}_{t_k} + \mathbf{R}_{t_k} \mathbf{x}_i^c(t_0) + S_{t_k} \mathbf{x}_i^c(t_0) + \sum_{p=1}^m o_{ip} H(t_k - t_{ip}^o) + \sum_{j=1}^n a_{ij} \sin\{w_{ij}(t_k - t_0) + \varphi_{ij}\} \quad (1)$$

and

$$\begin{aligned} \mathbf{x}_{GC}^s(t_k) + \mathbf{v}_{GC}^s(t_k) &= \mathbf{x}_{GC}^c(t_k) + \mathbf{T}_{t_k} \\ \mathbf{x}_p^s(t_k) + \mathbf{v}_{xp}^s(t_k) &= \mathbf{x}_p^s(t_k) + \mathbf{R}_{t_k}^Y \\ \mathbf{y}_p^s(t_k) + \mathbf{v}_{yp}^s(t_k) &= \mathbf{y}_p^c(t_k) + \mathbf{R}_{t_k}^X \\ \dot{\mathbf{x}}_p^s(t_k) + \mathbf{v}_{xpr}^s(t_k) &= \dot{\mathbf{x}}_p^s(t_k) \\ \dot{\mathbf{y}}_p^s(t_k) + \mathbf{v}_{ypr}^s(t_k) &= \dot{\mathbf{y}}_p^s(t_k) \\ LOD^s(t_k) + \mathbf{v}_{LOD}^s(t_k) &= LOD^c(t_k) \end{aligned} \quad (2)$$

where $\mathbf{x}_i^l(t_k)$, $\mathbf{x}_{GC}^l(t_k)$, $\mathbf{x}_p^l(t_k)$, $\mathbf{y}(t_k)$, $\dot{\mathbf{x}}_p^l(t_k)$, $\dot{\mathbf{y}}_p^l(t_k)$ and $LOD^l(t_k)$ with superscript of $l = s$ are coordinate vectors of station i , apparent geo-center motion parameters (GCMPs), and Earth rotation parameters (ERPs) of input daily observations, respectively, and these with superscript of $l = c$ are corresponding stacking estimates. $\mathbf{x}_i^c(t_0)$ and $\dot{\mathbf{x}}_i^c$ are initial coordinates and the velocity of station i at the reference epoch t_0 . $\mathbf{v}_i^s(t_k)$, $\mathbf{v}_{GC}^s(t_k)$, $\mathbf{v}_{xp}^s(t_k)$, $\mathbf{v}_{yp}^s(t_k)$, $\mathbf{v}_{xpr}^s(t_k)$, $\mathbf{v}_{ypr}^s(t_k)$ and $\mathbf{v}_{LOD}^s(t_k)$ are the residuals for the observations of daily position, GCMPs and ERPs. \mathbf{T}_{t_k} , \mathbf{R}_{t_k} and S_{t_k} denote the 3 translation, 3 rotation and 1 scale parameters of similarity transformation between the daily and the inner long term reference (i.e., stacking solution). o_{ip} is the discontinuity corrections of the coordinate series i at epoch t_{ip}^o , $H(t_k - t_{ip}^o)$ is the Heaviside step function. The periodic signals can be modeled in the deterministic functional model, and a_{ij} , w_{ij} and φ_{ij} are the amplitude, angular rate and initial phase of harmonic j with frequency f_j .

2.2.1. Data Preprocess

For the global stations with daily solutions collected from IGS, the longest time span is about 21 years. Blewitt et al. indicated that the estimates of velocity could be biased by the periodic signals in the position time series, special for the stations with a short time span, and the minimum data span was suggested for velocity solutions [30]. The stations with a data time span of less than 2 years were excluded from the daily solutions by using the Gauss elimination method for the normal equation. Moreover, the station with data gaps larger than 20% were also excluded in the final daily solutions stacking. The input daily combinations used to stack for a cumulative solution are always affected by the position/velocity discontinuities, which should be considered in the Equation (1). Most of the intermittent offsets are caused by seismic event and equipment changes, while the sources of some offsets are still unknown. Griffiths and Ray indicated that the velocity uncertainty could worsen by about 40% if the numbers of offsets in the time series doubles [21]. For the detection of offsets in position time series, different methods are applied by researchers and the manual approach outperforms the automated ones [20]. Since the authors focus on the effects of known offsets on noise analyses, the discontinuity information for the second reprocessed position time series is available from the IGS and was used directly as a priori information in this study.

It is crucial to reduce the time-correlated errors induced by post-seismic deformations (PSDs), which usually have nonlinear trajectories and can be fitted using logarithmic or exponential curves, or the superposition of these two parametric models [16]. In this study, the PSDs caused by major earthquakes were corrected by adopting the parametric models provided by Altamimi et al. [31].

In order to reduce the effects of outliers in the daily solutions on the noise analyses, the daily solutions were checked station by station for each component. After the corrections of PSDs, the position time series of each component were fitted. The annual and semiannual signals were parameterized in the deterministic model, and the discontinuity information was used. The observations with residuals larger than 5 cm or 5σ were deleted and an iterative process was applied until no outliers were detected. As a result, about 0.7% of observations were again eliminated and 647 stations (Figure 1) in total with daily solutions were used to obtain the cumulative solution.

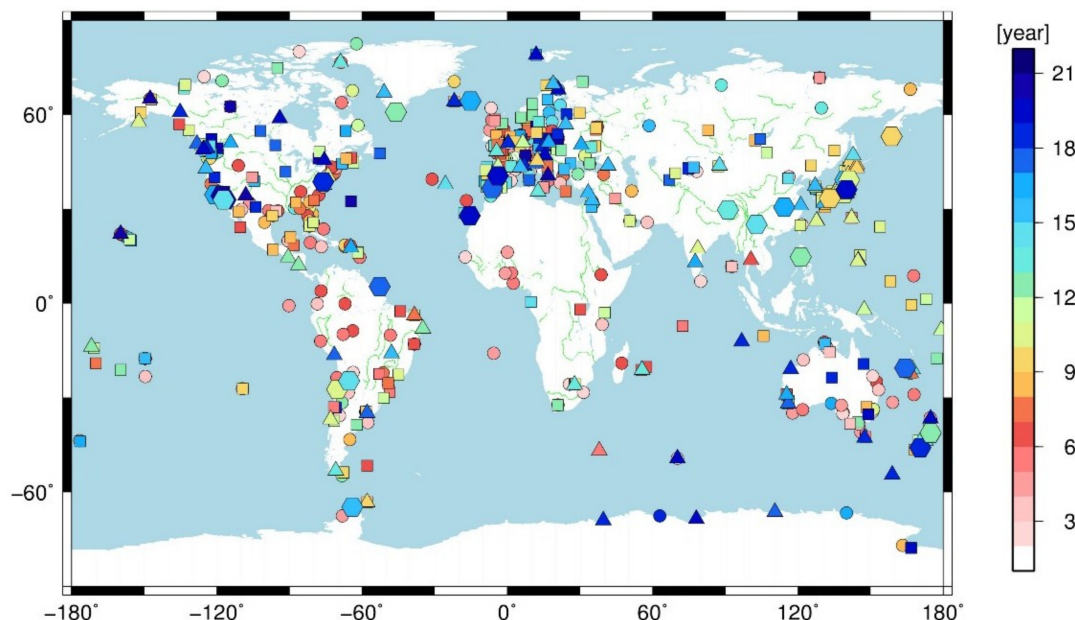


Figure 1. The global distributed stations with different observation time span and numbers of offset. Circle: no offsets found in the time series; square: 1–2 offsets; triangle: 3–4 offsets; hexagon: more than 4 offsets in the time series.

The average observation time span of all stations was about 10.2 years (Figure 1), the number of stations with time span larger than 5 years, 11 years, and 17 years were 533 (82%), 260 (40%), and 79 (12%), respectively. There were also 33 stations with observation time span of less than 3 years, and 14 stations with more than a 20-year time span for the position time series. For the selected stations, there were 403 stations with position/velocity offsets occurring in the time series and one offset occurs every 7.2 years on average.

2.2.2. Periodic Signals and Weight Matrix

The periodic signals in the GNSS position time series are not only the results of geodynamic mechanisms, but can also be caused by technique-related systematic errors and data processing strategies [12,14,32–34]. The periodic signals have impacts on both noise analysis and other parameter estimations. Since the unmodeled periodic signals could enhance the autocorrelation and appear to be flicker noise in the stochastic model, the significant signals, except the seasonal ones, were proposed to be modeled for noise analyses [11,35]. Blewitt et al. indicated that the velocity bias caused by the periodic signals in the position time series can be neglected when the observation time span is larger than 4.5 years and the minimum data span of 2.5 years is suggested for the velocity solution [30]. In this study, the effects of unmodeled periodic signals on noise analyses is assumed the same for the comparison of different stacking solutions, so only the annual and semiannual variations (i.e., seasonal signals) were considered in the deterministic model. Moreover, the authors focused on the effects of seasonal signals on noise analyses and no more periodic signals are considered in simulated GNSS position time series except the seasonal ones.

In order to assess the effects of weight matrices of observations on the noise analyses of the cumulative solution, the weight matrix derived from the covariance in the daily solution independent exchange (SINEX) files were used.

2.2.3. Data Simulation and Cumulative Solutions

Since it was difficult to assess the effects of offsets in a time series on noise analyses separately for the practical GNSS position time series, the simulated daily solutions were generated in this study. Using the simulated position time series, it was possible to obtain an assessment of effects of seasonal signals on the noise analyses. Moreover, the simulated data could cooperate with the real daily solutions to assess the effects of the weight matrix on the noise analyses.

Four cumulative solutions with the IGS second reprocessed daily solutions and three solutions stacked for the simulated position time series are summarized in Table 1. The annual and semiannual signals are parameterized in the functional model for all the seven cumulative solutions.

In order to assess the effects of the transformation parameters on the results of noise analyses, two stacking solutions were obtained with/without the transformation parameters considered in the functional model with the practical GNSS position time series (i.e., `igs_unit_none` vs `igs_unit_trs`). No more constraints except a loose constraint of 0.1 m were applied for the transformation parameters in the daily solution stacking. Moreover, the solution `igs_cova_none` was also stacked and compared with the solution `igs_unit_none` to assess the effects of the weight matrix on noise analyses. Using the practical GNSS position time series, the stacking solution with the Helmert transformation parameters and full covariance information considered was obtained (`igs_cova_trs`) to assess the combined effects of the weight matrix and transformation parameters on noise analyses.

Table 1. Cumulative solutions with different processing strategies for noise analyses. For the solutions with different labels, “sim” and “igs” mean the data sources, “sim” for simulated and “igs” for real IGS position time series; “unit” and “cova” mean the weight matrix used for cumulative solutions, “unit” stands for unit or identity matrix and “cova” means full weight matrix derived from the covariance information in the IGS daily solutions. For cumulative solutions using the simulated time series, the “real” and “none” mean offsets parameterized or not, respectively, in the functional model. For cumulative solutions using the real time series, where the “trs” and “none” mean transformation parameters estimated or not, respectively.

Data Source	Solution	Weight Matrix	Offsets/Transformation Parameters
Simulate position time series	sim_unit_none	unit matrix	No offsets
	sim_unit_real	unit matrix	Offsets information from IGS
	sim_cova_none	covariance	No offsets
IGS second reprocessed daily solutions	igs_unit_none	unit matrix	No transformation parameters
	igs_unit_trs	unit matrix	Translation, rotation, and scale
	igs_cova_none	covariance	No transformation parameters
	igs_cova_trs	covariance	Translation, rotation, and scale

The estimations of seasonal signals and the linear part in igs_cova_trs were used to simulate the position time series. A combination of a power law noise and white noise was also added to the simulated position time series. The spectral indexes of -0.5 ± 0.25 for simulated noise were assumed, which is comparable with the results of noise analyses in the study of Bogusz et al. [11]. Meanwhile, the amplitudes of power noise of 5.5 ± 1.5 and $12.0 \pm 5.0 \text{ mm}^{-k/4}$ for horizontal and vertical components, respectively, were assumed, which were derived from the noise analyses of igs_cova_trs and were almost as much as the flicker noise in the study of Williams et al. [9]. Meanwhile, the white noise with a Gaussian distribution of 1.0 ± 0.5 and $2.0 \pm 1.0 \text{ mm}$ for the horizontal and vertical, respectively, was also added to the position time series.

The final simulated position time series with noise were extracted from the continuous raw simulated time series to guarantee that the data sampling interval was the same as those of the real GNSS position time series, and the combined noise was estimated with free available Hector software [36]. The spectral indexes of power law noise of all stations in the final simulated position time series were -0.57 ± 0.17 , -0.45 ± 0.17 , and -0.55 ± 0.15 for the east, north, and up components, respectively. The amplitudes were 5.8 ± 1.9 , 5.1 ± 1.6 , and $12.1 \pm 3.3 \text{ mm}^{-k/4}$ for the corresponding components. The estimated amplitudes of white noise were 1.2 ± 0.6 , 0.5 ± 0.6 , and $2.0 \pm 1.0 \text{ mm}$ for the east, north, and up components, respectively.

For the three cumulative solutions derived from the simulated position time series, sim_unit_none was obtained by neglecting the correlations between stations (i.e., unit matrix used for observations) and no position/velocity offsets were considered in the deterministic model. In order to assess the effects of offsets in the GNSS position time series, offset parameters were added in the functional model using the discontinuity information from IGS (i.e., solution sim_unit_real). The simulated time series only included the stations' coordinates, and no Helmert transformation parameters were simulated and estimated in the cumulative solutions. As a result, it was easy to assess the effect of the weight matrix on the noise analyses by comparing sim_unit_none to sim_cova_none, and the solution sim_cova_none was obtained by considering the covariance information from the IGS second reprocessed daily solutions.

2.2.4. Noise Analyses for Residual Series

Generally, the noise in the GNSS position time series can be described as a power law (PL) process and has the form of a power spectrum [9]

$$P(f) = P_0 \left(\frac{f}{f_0} \right)^k \quad (3)$$

where f is the temporal frequency, P_0 and f_0 are normalized constants, and k is spectral index. Noises with a spectral index range from -3 to -1 are non-stationary processes, including the random walk (RW) process with $k = -2$. The special process with spectral index of -1 is called flicker noise (FN) and occurs in almost all electronic devices as a low-frequency phenomenon. Noises with spectral indexes of $-1 < k < 1$, including the special case with $k = 0$ called white noise (WN), are stationary processes whose unconditional joint probability distribution does not change when shifted in time.

There are several suggested methods to estimate the optimal noise model for the GNSS position time series. The power spectrum analysis (PSA) can be used to describe the stochastic processes distinctly by fitting the power at different frequencies with a linear function, and the noise type can be related to the slope. However, the limitation of the PSA is that the captured noise properties are not precise enough and not reliable for the low frequency band [4,7,37]. A more reliable technique is the maximum likelihood estimation (MLE), which is preferred by many researchers in noise analysis. To estimate the parameters in the stochastic models using MLE, the probability function (Equation (4)) with a Gaussian distribution assumption is maximized by adjusting the estimated parameters:

$$lik(\hat{\theta}, C_x) = \frac{1}{(2\pi)^{N/2} (\det C_x)} \exp\left(-0.5\hat{\theta}^T C_x^{-1} \hat{\theta}\right) \quad (4)$$

where $lik(*)$ is the likelihood function, \det is the determinant of a matrix, $\hat{\theta}$ is the post-fitting residuals between the observations and functional model, N is the length of position time series, and C_x is the observations covariance matrix. Since we assume the combination of white and power law noise in the time series, the C_x can be expressed as follows:

$$C_x = \sigma_{wn}^2 I + \sigma_{pl}^2 J_{pl}(k) \quad (5)$$

where σ_{wn}^2 and σ_{pl}^2 are the amplitudes of the white noise and power law noise, respectively. I is the identity or unit matrix, and $J_{pl}(k)$ denotes the covariance matrix of power law noise in the observation, which is correlated with the spectral index.

The disadvantage of MLE used in noise analyses is the heavy computational burden. In order to reduce the computation time and to compensate for missing data in the position time series, Bos et al. developed a fast MLE method, which had been applied in the Hector software [36]. Allan variance and Hadamard variance can also be used to analyze noise characteristics of position residuals to alleviate the computational burden [38,39]. In this study, the results of noise analyses were derived from the residuals of different cumulative solutions described in Section 2.2.3 using the Hector software. Since the removal of a trend from the position time series can reduce the power of the spectral estimates significantly, a linear part was subtracted from the simulated noise series and the residuals of different solutions during noise analyses. The authors limited the focus on the power law noise comparison between different strategies.

3. Results

The results of the noise analyses are given in this section for both the simulated GNSS position time series and the practical data. The effect of the weight matrix, offsets, seasonal signals, and transformation parameters on the noise properties are analyzed in detail.

3.1. Effect of Seasonal Signal on Noise Analyses

It is widely known that the seasonal signals in the GNSS position time series are mostly related to the Earth surface mass redistribution including atmospheric, non-tidal oceanic, and hydrological loading deformations. In order to assess the effects of seasonal signals on noise properties in the position time series, Figure 2 demonstrates the difference of power law noise between the estimation of simulated noise and the results from `sim_unit_none`.

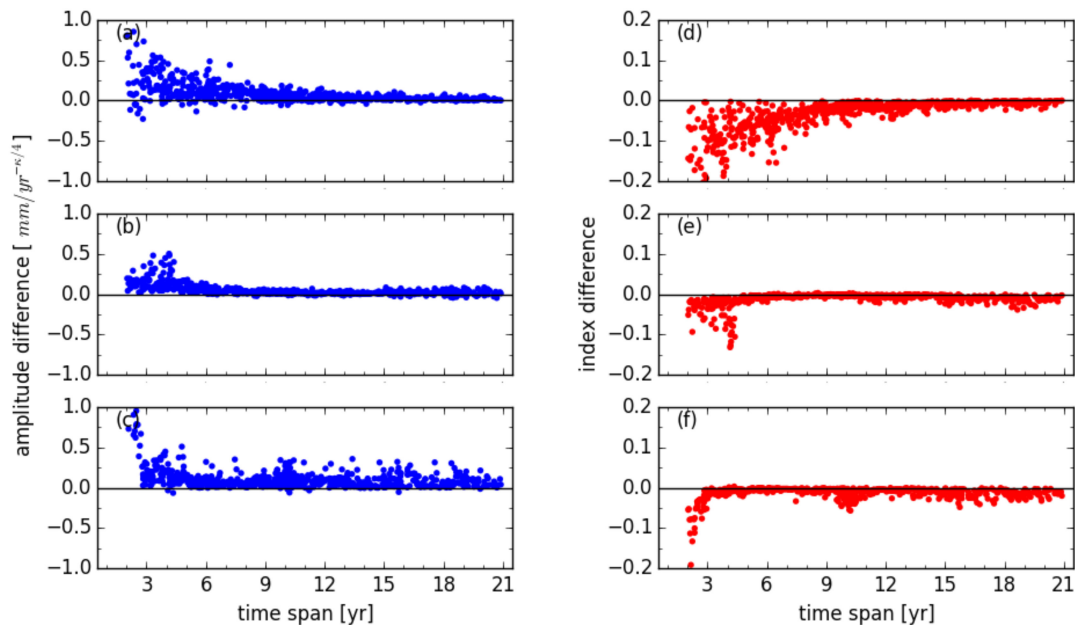


Figure 2. Noise difference between simulated noise and those derived from solution `sim_unit_none` for amplitudes (left panel) and spectral indexes (right panel) of power-law noise, with (a,d) for the east, (b,e) for the north, and (c,f) for the vertical component.

There were 597 (91.2%), 597 (92.3%), and 632 (97.7%) of 647 stations with a smaller amplitude for `sim_unit_none` for the east, north, and up component, respectively. The median values of amplitude differences between the estimation of simulated noise and `sim_unit_none` were 0.05, 0.03 and 0.08 $\text{mm}^{-k/4}$. There were also 73, 24, and 93 stations with amplitude differences larger than 0.2 $\text{mm}^{-k/4}$ for the three components. With the increasing observation time span, the differences of amplitudes and spectral indexes are decreased and become stable.

Compared with the simulated noise, there were only 3 (0.5%), 8 (1.2%), and 6 (0.9%) stations with lower spectral indexes for `sim_unit_none`. For the spectral indexes, the median values of differences between estimated noise simulation and `sim_unit_none` were -0.02 , -0.01 , and -0.01 for east, north, and up components, respectively. There were also 59, 5, and 5 stations with spectral indexes differences larger than 0.1 for the three components. For the east component, more stations with a large spectral indexes difference may be related to the smaller amplitude of the annual signal. There were 164 stations with an observation time span of less than 6 years, and the median amplitudes of the annual signal were 0.6, 1.1, and 3.1 mm for the east, north, and up components, respectively. Compared with the amplitudes of north and up components, there were 75% and 92% stations with a smaller annual amplitude for east component, respectively. Considering the amplitudes of the simulated power law noise in the simulated observations, the results of the noise analyses of the east component seems to be more easily affected by seasonal signals, which needs further validation in the future.

Since no colored noise model was assumed in the generation of cumulative solutions, the systematic bias for the amplitudes and spectral indexes shown in Figure 2 should be induced by the existence and estimation of seasonal signals in the deterministic model. Bosugz et al. also validated that the power law amplitudes decreased, and the spectral indexes were much “whiter” when all periodicities are subtracted from the position time series [11].

The differences of the annual amplitude and phase, between the raw simulated annual signal and estimation of solution `sim_unit_none`, are shown in Figure 3. The amplitude difference of the up component was more scattered than the horizontal components, which is consistent with the larger amplitude difference of power law noise. The median values of the annual amplitude absolute difference were 0.15 ± 0.20 , 0.09 ± 0.15 , and 0.26 ± 0.37 mm for the east, north, and up components, respectively. Meanwhile, the median values for annual phase absolute difference were 11.52 ± 32.65 ,

5.40 ± 18.20 , and 4.68 ± 18.80 degrees for the corresponding components. It is also noticed that the amplitude and phase differences of annual signal decreased with the increasing observation time span for the horizontal components.

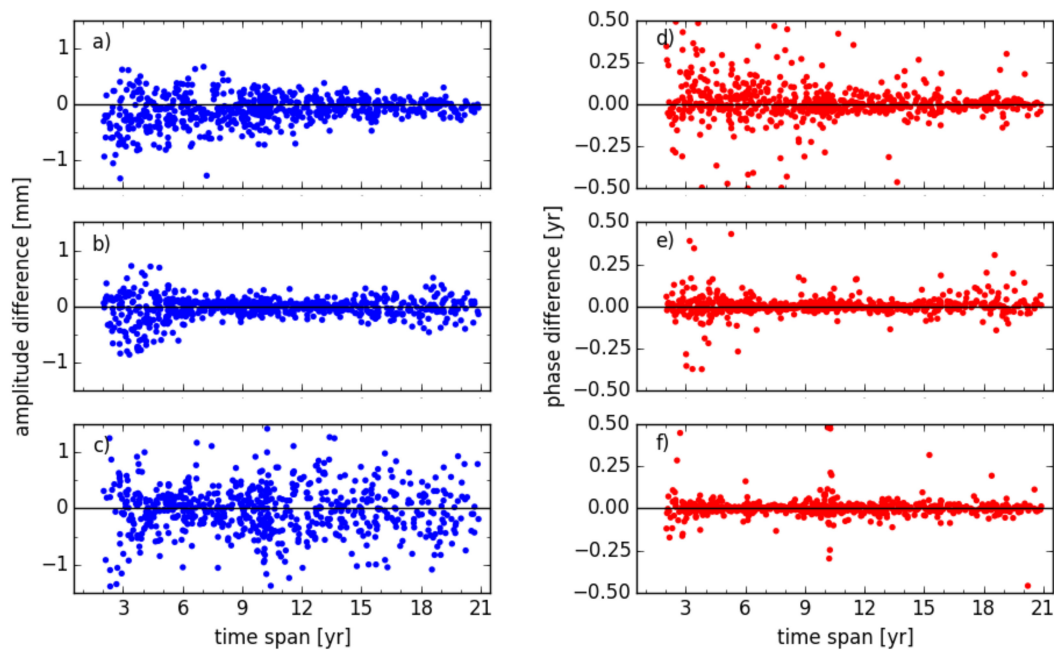


Figure 3. Difference of annual signal between simulated and those derived from the solution `sim_unit_none` for amplitudes (**left panel**) and phase (**right panel**), with (**a,d**) for the east, (**b,e**) for the north, and (**c,f**) for the vertical component.

3.2. Effect of the Weight Matrix on Noise Analyses

Both the simulated and real position time series were used to assess the effect of weight on the noise analyses of residuals. Figure 4 shows the comparison of the noise analyses between `sim_unit_none` and `sim_cova_none`. Since no offsets were simulated in the position time series and no Helmert transformation parameters modeled in the deterministic model, the differences of noise properties could be attributed to the weight matrix used for the observations. Compared to the solution without considering the spatial correlation (i.e., `sim_unit_none`), the noise of `sim_cova_none` with a full weight matrix seemed to more “colored”. There were 643 (99.4%), 646 (99.8%), and 630 (98.4%) stations for `sim_cova_none` with lower spectral indexes for east, north, and up components, respectively. The median values of the spectral indexes difference were 0.02, 0.01, and 0.01 for the three components. Moreover, there were 64, 57, and 35 stations with a spectral indexes difference larger than 0.1 for the east, north, and up components, respectively.

For the amplitude of the power law noise, there were 598 (92.4%), 602 (93%), and 616 (95.2%) stations for `sim_cova_none` with a larger amplitude than `sim_unit_none` for the east, north, and up components, respectively. The median values of amplitude difference were -0.05 , -0.06 , and $-0.04 \text{ mm}^{-k/4}$ for the three components. From the comparison of the noise analyses between `sim_unit_none` and `sim_cova_none`, it indicated that the spatial correlation derived from the covariance information could induce the shift toward flicker noise and enhance the amplitudes of colored noise.

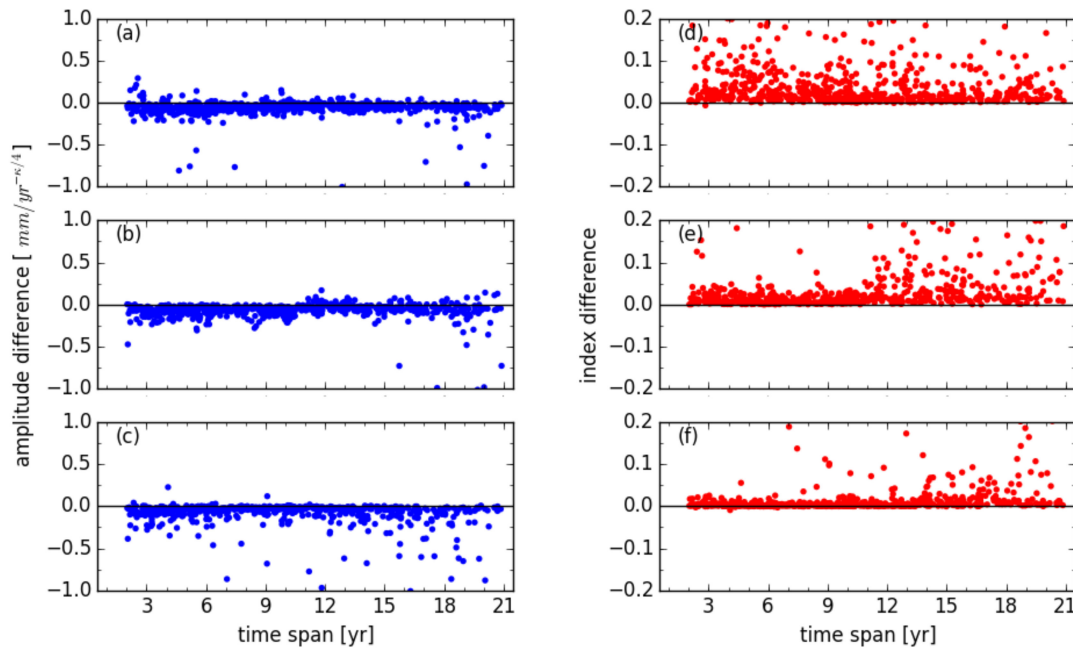


Figure 4. Noise difference between the solution `sim_unit_none` and `sim_cova_none` for amplitudes (**left panel**) and spectral indexes (**right panel**) of power-law noise, with (**a,d**) for the east, (**b,e**) for the north, and (**c,f**) for the vertical component.

Table 2 lists the statistical results of the annual amplitude and phase differences between the simulated annual signal and the estimation from different solutions. Compared with the simulated annual signal, both the amplitude and phase difference of the annual signal derived from `sim_cova_none` were more scattered than `sim_unit_none`. The absolute biases of the annual amplitude of `sim_unit_none` were 0.15, 0.09, and 0.26 mm for the east, north, and up components, respectively. While the median values of `sim_cova_none` were 1.5 times larger than the ones of `sim_unit_none` for each component. This indicates that both the noise characteristics and annual signal could be changed when the spatial correlation between different stations in the stacking solution was considered using the covariance information. Since the position time series of different stations could be affected by each other when the correlations were considered, the abnormal observations, such as the offsets and outliers in the position time series, should be checked carefully.

Table 2. Maximum and median values with the standard deviation (SD) of the annual amplitude and phase absolute difference between the raw simulated and solution `sim_unit_none` and `sim_cova_none`. Unit: mm and degree for amplitude and phase, respectively.

Solution	Component	Amplitude		Phase	
		MAX	MED	MAX	MED
<code>sim_unit_none</code>	East	1.64	0.15 ± 0.20	179.64	11.52 ± 32.65
	North	0.86	0.09 ± 0.15	154.80	5.40 ± 18.20
	Up	3.77	0.26 ± 0.37	176.04	4.68 ± 18.80
<code>sim_cova_none</code>	East	1.77	0.23 ± 0.26	175.68	15.84 ± 35.60
	North	1.99	0.14 ± 0.22	162.70	11.52 ± 24.28
	Up	5.97	0.37 ± 0.63	169.56	6.12 ± 17.88

Using the practical IGS reprocessed daily solutions, the effect of different weight matrices could be assessed further. Figure 5 shows the difference in power law noise between `igs_unit_none` and `igs_cova_none`. Considering the full weight matrix from the covariance information, a shift towards more “colored” noise was also found, which is similar to the simulation case. There were 621 (96%),

632 (97.7%), and 491 (91.3%) stations with lower spectral indexes for igs_cova_none for the east, north, and up components, respectively. The median values of the spectral indexes difference between igs_unit_none and igs_cova_none were 0.02, 0.03, and 0.01 for the three components.

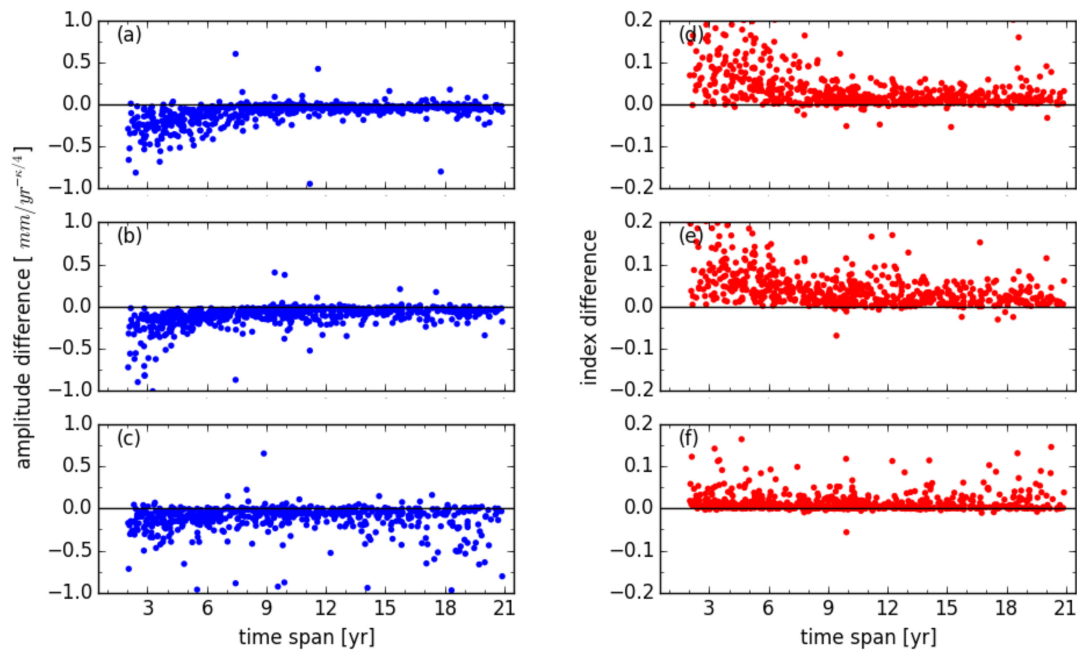


Figure 5. Difference between the solution igs_unit_none and igs_cova_none for the amplitudes (**left panel**) and spectral indexes (**right panel**) of the power-law noise, with (a,d) for the east, (b,e) for the north, and (c,f) for the vertical component.

It was also noticed that the spectral indexes difference decreased with the increasing observation time span, especially for the horizontal components, which was not similar to the results of simulation. For the stations with a time span of less than 8 years, the difference could even reach 0.2 or more. There were 74, 67, and 15 stations with spectral indexes difference larger than 0.1 for the east, north, and up components, respectively. For the amplitude of the power law noise, there were 605 (93.5%), 627 (96.9%), and 583 (90.1%) stations of igs_cova_none with larger amplitudes for the east, north, and up components, respectively. The median values of the amplitude difference were -0.05 , -0.08 , and $-0.06 \text{ mm}^{-k/4}$ for the three components.

3.3. Effect of Offset on Noise Analyses

In order to assess the effects of offsets in the position time series on noise characteristics, sim_unit_real was obtained by adding offset parameters in the functional model with the discontinuity information from the IGS for the 403 stations. It was clear that the additional offsets parameterized in the deterministic model could reduce the colored noise (Figure 6), where the numbers of stations with spectral indexes closer to zero were 379 (94.0%), 378 (93.8%), and 382 (94.8%) for the east, north, and up components, respectively. Meanwhile, 295 (73.2%), 319 (79.2%), and 343 (85.1%) stations of sim_unit_real had a smaller amplitude of power law noise than sim_unit_none for the three components. It was also found that the more offsets in the position time series, the lower the spectral indexes difference that were obtained. However, this does not mean that more offsets were encouraged to be parameterized in the deterministic model to have much “whiter” noise. Instead of over-parameterization for the offsets in the position time series, it was much wiser to check the consistency of noise characteristics between the pieces before and after the offsets happening and decide whether to process the pieces together [16,17,21].

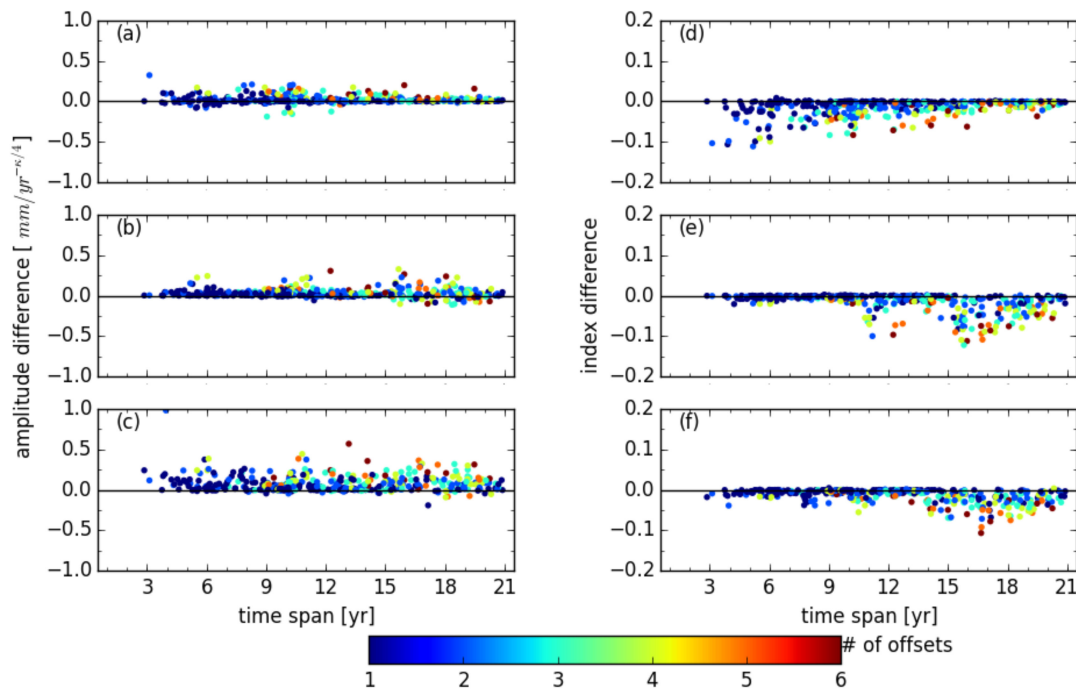


Figure 6. Noise difference between the solution `sim_unit_none` and `sim_unit_real` for amplitudes (**left panel**) and spectral indexes (**right panel**) of the power-law noise, with (a,d) for the east, (b,e) for the north, and (c,f) for the vertical component. The number of offsets in the position time series is shown with different colors.

Although the noise properties in the position time series could be changed by the intermittent offsets, the annual signal differences induced by the offsets were not significant. The median values of the annual amplitude absolute difference between `sim_unit_none` and `sim_unit_real` were 0.01 ± 0.03 , 0.01 ± 0.02 , and 0.03 ± 0.06 mm for the east, north, and up components, respectively. For the annual phase, the median values of the absolute difference between `sim_unit_none` and `sim_unit_real` were 0.72 ± 3.60 , 0.72 ± 2.94 , and 0.36 ± 2.76 degrees for the three components.

3.4. Effect of Helmert Transformation Parameters on Noise Analyses

The solutions with and without Helmert transformation parameters (three translation, three rotation, and one scale parameters) considered in the functional model were obtained and compared. Figure 7 demonstrates the difference of power law noise between `igs_unit_none` and `igs_unit_trs` for the selected stations. For the spectral indexes, `igs_unit_none` had 474 (73.3%), 451 (69.7%), and 426 (65.8%) stations with lower spectral indexes for the east, north, and up component, respectively. A clear spatial dependence was noticed for the stations with more “colored” noise (i.e., lower spectral indexes) for `igs_unit_trs`, especially for the north and up components. For the north component, the inner continental stations in Asian areas for `igs_unit_trs` mostly have lower spectral indexes than `igs_unit_none`. For the up component, besides the stations in this inner continental region in Asia, the stations along the Antarctic and Baffin Bay coastline also showed lower spectral indexes for `igs_unit_trs`.

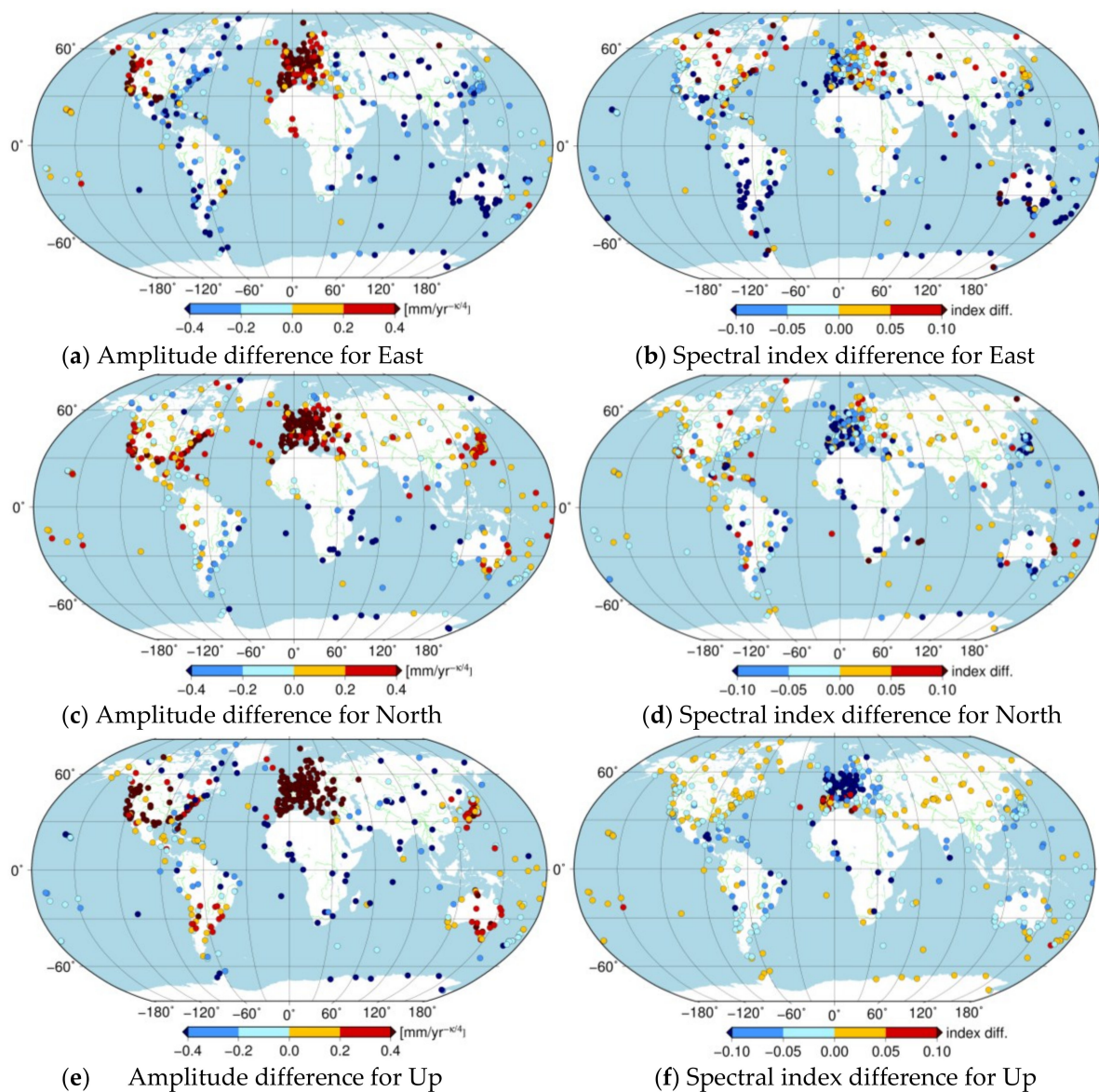


Figure 7. Amplitudes and spectral indexes differences between the solution `igs_unit_none` and `igs_unit_trs` for the global distributed stations.

For the amplitude difference of power law noise between `igs_unit_none` and `igs_unit_trs`, there were 287 (45.4%), 458 (70.8%), and 431 (66.6%) stations with a larger amplitude for `igs_unit_none` for the east, north, and up components, respectively. Moreover, the stations with an amplitude difference larger than $0.4 \text{ mm}^{-k/4}$ were mainly situated within the Europe area. Collilieux et al. indicated that estimating the transformation parameters over the whole network could alias the loading signals into the position time series [40]. Here the authors validated that these additional parameters in the deterministic model could also induce systematic biases for the colored noise with different regional patterns and should be considered carefully [19,31].

3.5. Combined Effect of Helmert Transformation Parameters and Weight Matrix on Noise Analyses

It was possible to assess the combined effect of Helmert transformation parameters and weight matrix on the noise analyses of the practical position time series through the comparison between `igs_unit_none` and `igs_cova_trs`. Considering the transformation parameters and full weight matrix derived from the covariance information, the noise of the solution `igs_cova_trs` showed different characteristics for the horizontal and up components. There were 471 (72.8%) and 499 (77.1%) stations

for `igs_cova_trs` with lower spectral indexes for the east and north components, respectively. For the up component, there were only 249 (38.6%) stations with more “colored” noise (i.e., lower spectral indexes) for this solution. The stations with a different performance in the noise analyses for up component were mainly situated in the Europe area (Figure 8). Klos et al. found a strong impact of the Baltic Sea on the position residuals of stations located in the Europe area and lower spectral indexes of the up component for stations in this area were obtained [41]. Since the dense stations were located in the Europe area, this may result in colored noise that can be reduced significantly by the transformation parameters (especially the scale parameter) for the stations located in this area. The median values of spectral indexes between `igs_unit_none` and `igs_cova_trs` were 0.02, 0.02 and -0.01 for the east, north, and up components, respectively. Meanwhile, there were also 76, 63, and 117 stations with absolute spectral indexes larger than 0.1 for the three components.

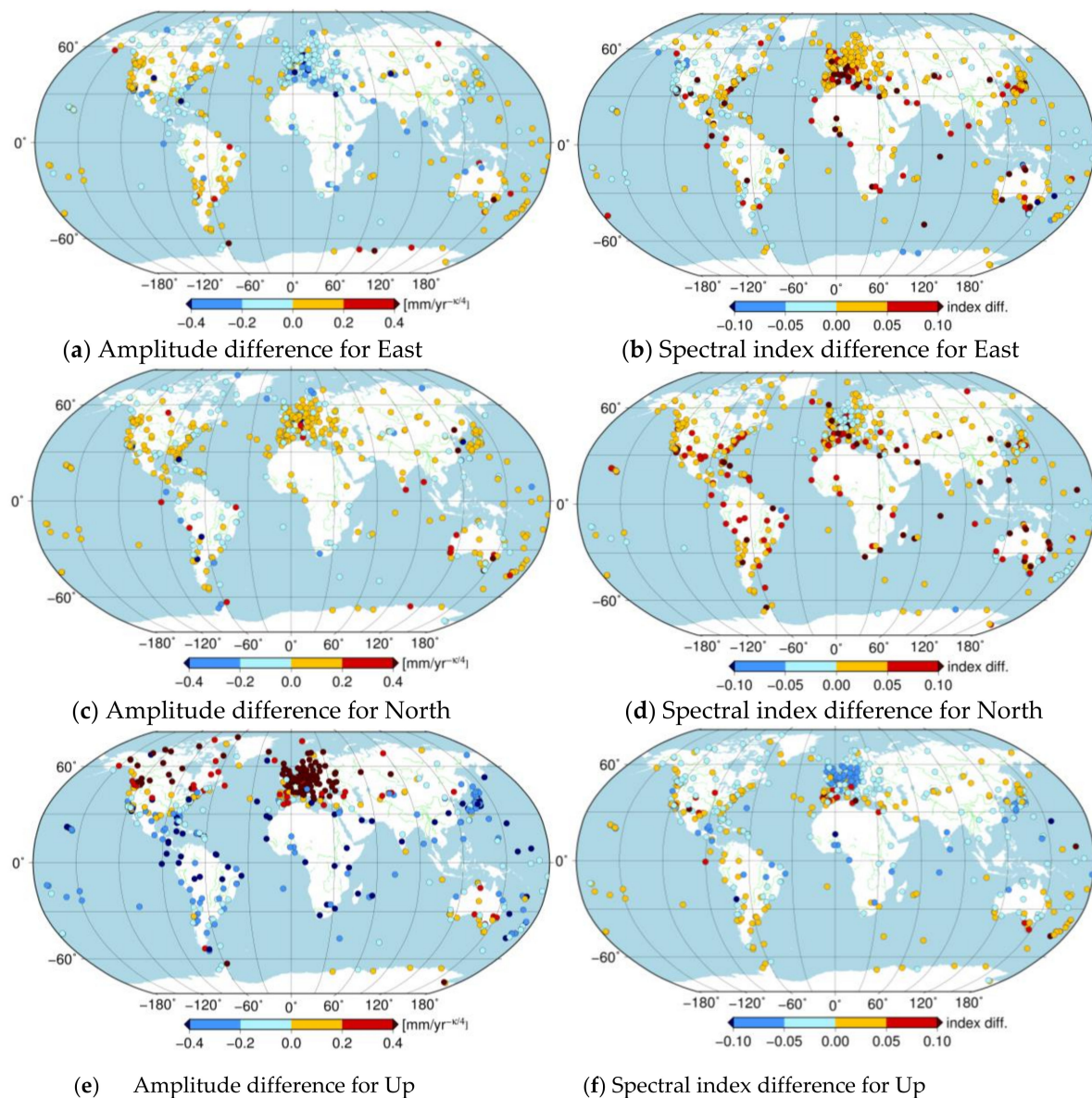


Figure 8. Amplitudes and spectral indexes differences between the solution `igs_unit_none` and `igs_cova_trs` for the global distributed stations.

For the amplitude difference of the power law noise, there was no systematic bias between `igs_unit_none` and `igs_cova_trs`, and there were 382 (59.0%), 235 (36.3%), and 337 (52.1%) stations for the solution `igs_cova_trs` with a larger amplitude for the east, north and up components, respectively.

However, significant amplitude differences were found for stations located in the Europe area and near the equator. Moreover, there were 14, 15, and 249 stations with absolute amplitude differences larger than $0.4 \text{ mm}^{-k/4}$ for the three components.

Figure 9 demonstrates the difference of the power law noise between `igs_unit_none` and `igs_cova_trs` over the observation time span. The spectral indexes differences for the stations with a time span of less than 8 years seemed to be more scattered than the other stations, especially for the horizontal components. A similar phenomenon was also noticed for the amplitude difference between `igs_unit_none` and `igs_cova_trs`.

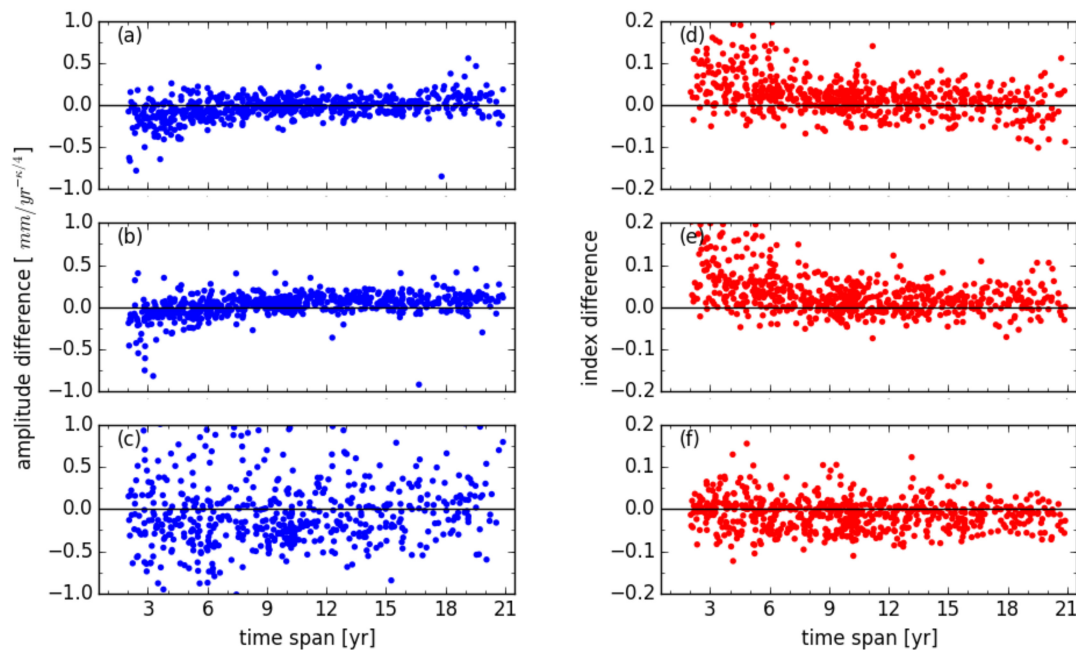


Figure 9. Noise difference between the solution `igs_unit_none` solution `igs_cova_trs` for amplitudes (**left panel**) and spectral indexes (**right panel**) of the power law noise, with (a,d) for the east, (b,e) for the north, and (c,f) for the vertical component.

Comparing the results of the noise analyses in Section 3.2, Section 3.4 and this section, it was found that the effects of the weight matrix and Helmert transformation parameters on the noise analyses showed different patterns. For most stations selected in this study, the weight matrix could enhance the colored noise, while the estimated transformation parameters were able to reduce the colored noise. When the two factors were considered together to obtain the stacking solution `igs_cova_trs`, a new pattern was again shown for the noise analyses, which could be contributed to the combined effects of the weight matrix and transformation parameters. For the horizontal components of the solution `igs_cova_trs`, the power law noises of global stations were mainly affected by the weight matrix, which had lower spectral indexes for most stations. However, the transformation parameters estimated in the functional model had more of an impact than the weight matrix on the power law noise for the up component. As a result, the transformation parameters, especially for the scale parameter, shifted the noise of the solution `igs_unit_none` toward much “whiter”.

4. Discussions

It is critical to have good knowledge about the noise characteristics in the GNSS position time series to obtain reliable velocity uncertainty, and assuming the only white noise in the position time series always overestimates the uncertainty of rate. Using the simulated and real GNSS position time series in this study, cumulative solutions with a least squares method and different strategies were obtained. The parameters of the power law noise plus white noise were then estimated for the residuals from different stacking strategies. The authors then assessed the effects of seasonal signals, the weight

matrix used for observation, offsets in GNSS time series, and Helmert transformation parameters on the noise analyses of the residuals. Table 3 summarizes the effects of variable factors on the noise of the residuals.

Table 3. Effects of different variable factors on the noise analyses for the residuals of stacking solutions with different strategies. The columns of “Amplitude” and “Spectral Index” list the percentage of stations with smaller or lower values for the latter solution in column “Test”. The values in the parenthesis are the medians of absolute difference between the two solutions in column “Test”.

Variable Factor	Test	Comp.	Amplitude	Spectral Index
Seasonal signals	simuation vs. sim_unit_none	East	91.2% (0.05)	0.5% (0.02)
		North	92.3% (0.03)	1.2% (0.01)
		Up	97.7% (0.08)	0.9% (0.1)
Weight matrix	sim_unit_none vs. sim_cova_none	East	7.6% (0.05)	99.4% (0.02)
		North	7.0% (0.06)	99.8% (0.01)
		Up	4.8% (0.04)	98.4% (0.01)
	igs_unit_none vs. igs_cova_none	East	6.5% (0.06)	96.0% (0.02)
		North	3.1% (0.08)	97.7% (0.03)
		Up	9.9% (0.07)	91.3% (0.01)
Offsets	sim_unit_none vs. sim_unit_real	East	73.2% (0.01)	6.0% (0.01)
		North	79.2% (0.02)	6.2% (0.01)
		Up	85.1% (0.05)	5.2% (0.01)
Transformation parameters	igs_unit_none vs. igs_unit_trs	East	45.4% (0.33)	26.7% (0.06)
		North	70.8% (0.26)	31.3% (0.04)
		Up	66.6% (0.43)	34.2% (0.03)
Transformation parameters and weight matrix	igs_unit_none vs. igs_cova_trs	East	41.0% (0.8)	72.8% (0.03)
		North	63.7% (0.08)	77.1% (0.03)
		Up	47.9% (0.30)	38.6% (0.02)

From the comparison of effects on noise analyses related to different variable factors (Table 3), the largest impact on the power law noise was induced by the Helmert transformation parameters, which could reach $0.5 \text{ mm}^{-k/4}$ and 0.1 for the medians of amplitude and spectral index, respectively. For simplicity, a flicker noise with an amplitude of $1 \text{ mm}^{1/4}$ was assumed for the position time series with a 10-year time span, then the bias of the noise characteristics related to transformation parameters could cause an error of velocity of about 0.05 mm/yr, which should be taken into account for the increasing demand of high-precision velocity of 0.1 mm/yr [42]. Moreover, the impact could be enlarged for stations with a shorter time span. For other factors, the effects on velocity uncertainty may be about 0.01 mm/yr when the noise estimation from the post residuals were used as a priori information. Further study is also needed to assess the effects on velocity estimations in detail but is out of the scope of this paper. Blewitt indicated that there is an equivalence between the deterministic model and stochastic model in the parameter adjustment, the unmodeled functional part could be shown in the stochastic and vice versa [43]. Any inconsistencies between the deterministic and stochastic model can cause overestimation or underestimation for the parameters in both models. However, the accurate deterministic model was used for the simulated time series, but the power law noise of post residuals could still be biased from the a priori known noise information.

Fritsche et al. indicated that the contribution of GLONASS becomes considerable starting with the year 2008 for GNSS-related parameters (e.g., stations coordinates, Earth rotation pole parameters) [44]. Distinct peaks were found at periods of 7.8 and 8.2 days in the position time series for analysis centers with GLONASS data processed in the second reprocess, which was close to the nominal ground period of the GLONASS satellite (8 days) [29,45]. When all significant periodic signals in position time series were considered, Bogusz and Klos indicated that the noise should be closer to white noise [11]. Further comparison would be done for noise analysis of station position time series using GPS and GPS/GLONASS data.

5. Conclusions

Previous studies estimated the noise properties in the GNSS position time series and always took the annual and semi-annual signal into account in the functional model. However, they had seldom assessed the effect of the seasonal signal on the noise analyses. Compared with the simulated annual signal and noise, the mutual effects of seasonal signals and noise properties on each other were assessed in this study. Estimating the seasonal signals in the deterministic model resulted in much “whiter” noise for more than 98% of stations. For stations with an observation time span of less than 6 years, the spectral indexes difference could even reach 0.2. Meanwhile, the noise in the simulated position time series could also induce a median bias of 0.26 mm for the annual signal of the up component.

Using the current discontinuity information for GNSS position time series contributing to the ITRF2014, the effects of position/velocity offsets in simulated time series on the power law noise were assessed. The parameterization of the irregular offsets could induce spectral indexes closer to zero and smaller amplitudes for power law noise.

The effect of the weight matrix on noise analyses was assessed using the simulation as well as IGS second reprocessed solutions. The comparison indicated that the weight matrix derived from the covariance information could enhance the colored noise for more than 90% of stations. Moreover, using the simulated data, the median biases of the annual amplitude caused by different weight matrices could reach 0.2 and 0.4 mm for the horizontal and up components, respectively. When the additional Helmert transformation parameters were considered in the deterministic model, the colored noise of about 70% of stations were weakened for the three components, and a regional characteristic was also noticed for the spectral indexes difference. Finally, the transformation parameters and full weight matrix could result in 75% of stations with lower spectral indexes for the horizontal components. However, the percentage was only 40% for the up component, which indicated that weight matrix was the dominant factor for horizontal components while the transformation parameters were the dominant ones for vertical component. In order to obtain a velocity precision of 0.1 mm/yr for high-precision and long-term Earth science applications, the authors suggested that the Helmert transformation parameters should be considered carefully in the stacking model of position time series. Although the systematic bias could be caused by offsets and the weight matrix for the colored noise, the impacts of these systematic errors on velocity could be neglected.

Author Contributions: G.C. collected the data in this study, performed the data analysis, and wrote the paper. Q.Z. and N.W. edited the manuscript and provided valuable comments on the designed tests. J.L. provided the research interest and some valuable insights. All authors discussed the results and implications and commented on the manuscript at all stages.

Funding: The paper was accomplished with the financial support of the National Natural Science Foundation of China projects with No. 41774007 and 41774035. The work was also partly supported by the State Key Research and Development Programme of China (No. 2016YFB0501802).

Acknowledgments: We thank IGS for the second reprocessed terrestrial reference daily solutions with time span of over 20 years. We also thank the anonymous reviewers for their comments that helped to improve the manuscript.

Conflicts of Interest: The authors declare no conflict of interest.

References

1. Kusche, J.; Schrama, E.J.O. Surface mass redistribution inversion from global GPS deformation and Gravity Recovery and Climate Experiment (GRACE) gravity data. *J. Geophys. Res. Solid Earth* **2005**, *110*, 117–134. [[CrossRef](#)]
2. Dmitrieva, K.; Segall, P.; DeMets, C. Network-based estimation of time-dependent noise in GPS position time series. *J. Geod.* **2015**, *89*, 591–606. [[CrossRef](#)]
3. Williams, P.S.D. The effect of coloured noise on the uncertainties of rates estimated from geodetic time series. *J. Geod.* **2003**, *76*, 483–494. [[CrossRef](#)]

4. Langbein, J.; Johnson, H. Correlated errors in geodetic time series: Implications for time-dependent deformation. *J. Geophys. Res. Solid Earth* **1997**, *102*, 591–604. [[CrossRef](#)]
5. Zhang, J.; Bock, Y.; Johnson, H.; Fang, P.; Williams, S.; Genrich, J.; Wdowinski, S.; Behr, J. Southern California permanent GPS geodetic array: Error analysis of daily position estimates and site velocities. *J. Geophys. Res. Atmos.* **1997**, *102*, 18035–18055. [[CrossRef](#)]
6. Wang, W.; Zhao, B.; Wang, Q.; Yang, S. Noise analysis of continuous GPS coordinate time series for CMONOC. *Adv. Space Res.* **2012**, *49*, 943–956. [[CrossRef](#)]
7. Mao, A.; Harrison, C.G.A.; Dixon, T.H. Noise in GPS coordinate time series. *J. Geophys. Res.* **1999**, *104*, 20. [[CrossRef](#)]
8. Santamaria-Gomez, A.; Bouin, M.N.; Collilieux, X.; Wöppelmann, A.G. Correlated errors in GPS position time series: Implications for velocity estimates. *J. Geophys. Res.* **2011**, *116*. [[CrossRef](#)]
9. Williams, S.D.P.; Bock, Y.; Fang, P.; Jamason, P.; Nikolaidis, R.M.; Prawirodirdjo, L.; Miller, M.; Johnson, D.J. Error analysis of continuous GPS position time series. *J. Geophys. Res. Solid Earth* **2004**, *109*. [[CrossRef](#)]
10. Amiri-Simkooei, A.R.; Tiberius, C.C.J.M.; Teunissen, P.J.G. Assessment of noise in GPS coordinate time series: Methodology and results. *J. Geophys. Res. Solid Earth* **2007**, *112*, 141–158. [[CrossRef](#)]
11. Bogusz, J.; Klos, A. On the significance of periodic signals in noise analysis of GPS station coordinates time series. *GPS Solut.* **2016**, *20*, 655–664. [[CrossRef](#)]
12. Dong, D.; Fang, P.; Bock, Y.; Cheng, M.K.; Miyazaki, S. Anatomy of apparent seasonal variations from GPS-derived site position time series. *J. Geophys. Res. Atmos.* **2002**, *107*. [[CrossRef](#)]
13. Tregoning, P.; Watson, C. Atmospheric effects and spurious signals in GPS analyses. *J. Geophys. Res.* **2009**, *114*, 5493–5511. [[CrossRef](#)]
14. Xu, X.; Dong, D.; Fang, M.; Zhou, Y.; Wei, N.; Zhou, F. Contributions of thermoelastic deformation to seasonal variations in GPS station position. *GPS Solut.* **2017**, *21*, 1265–1274. [[CrossRef](#)]
15. Williams, S.D.P. Offsets in Global Positioning System time series. *J. Geophys. Res. Atmos.* **2003**, *108*, 211–227. [[CrossRef](#)]
16. Hackl, M.; Malservisi, R.; Hugentobler, U.; Jiang, Y. Velocity covariance in the presence of anisotropic time correlated noise and transient events in GPS time series. *J. Geodyn.* **2013**, *72*, 36–45. [[CrossRef](#)]
17. Liao, H.; Rui, X.U.; Chen, W.F.; Chen, C.; Tie, G.U. Statistical Analysis of Noise in GPS Time Series of Sichuan Province before and after the 2008 Wenchuan Earthquake. *Chin. J. Geophys.* **2013**, *56*, 160–169.
18. Jiang, W.; Deng, L.; Li, Z.; Zhou, X.; Liu, H. Effects on noise properties of GPS time series caused by higher-order ionospheric corrections. *Adv. Space Res.* **2014**, *53*, 1035–1046. [[CrossRef](#)]
19. Chen, G.; Zhao, Q.; Wei, N.; Li, M. Effect of Helmert Transformation Parameters and Weight Matrix on Seasonal Signals in GNSS Coordinate Time Series. *Sensors* **2018**, *18*, 2127. [[CrossRef](#)] [[PubMed](#)]
20. Julien, G.; Simon, W.; Matt, K.; Machiel, B.; Rolf, D.; Manoj, D.; Moore, A.W.; Ostini, L.; Petrie, E.; Roggero, M.; et al. Detecting offsets in GPS time series: First results from the detection of offsets in GPS experiment. *J. Geophys. Res. Atmos.* **2013**, *118*, 1–11.
21. Griffiths, J.; Ray, J. (Eds.) *Impacts of GNSS Position Offsets on Global Frame Stability*; EGU General Assembly: Vienna, Austria, 2015.
22. Yuan, L.G.; Ding, X.L.; Chen, W.; Simon, K.; Chan, S.B.; Huang, P.S.; Chau, K.T. Characteristics of Daily Position Time Series from the Hong Kong Gps Fiducial Network. *Chin. J. Geophys.* **2008**, *51*, 976–990. [[CrossRef](#)]
23. Beutler, G.; Kouba, J.; Springer, T. Combining the orbits of the IGS Analysis Centers. *Bull. Géod.* **1995**, *69*, 200–222. [[CrossRef](#)]
24. Beutler, G.; Moore, A.; Mueller, I. The international global navigation satellite systems service (IGS): Development and achievements. *J. Geod.* **2009**, *83*, 297–307. [[CrossRef](#)]
25. Kouba, J. A simplified yaw-attitude model for eclipsing GPS satellites. *GPS Solut.* **2009**, *13*, 1–12. [[CrossRef](#)]
26. Dilssner, F.; Springer, T.; Gienger, G.; Dow, J. The GLONASS-M satellite yaw-attitude model. *Adv. Space Res.* **2011**, *47*, 160–171. [[CrossRef](#)]
27. Rodriguez-Solano, C.; Hugentobler, U.; Steigenberger, P. *Earth Radiation Pressure Model for GNSS Satellites*; EGU General Assembly: Vienna, Austria, 2011.
28. Petit, G.; Luzum, B. IERS Conventions (2010). *IERS Tech. Note* **2010**, *36*, 1–95.
29. Rebischung, P.; Altamimi, Z.; Ray, J.; Garayt, B. The IGS contribution to ITRF2014. *J. Geod.* **2016**, *90*, 611–630. [[CrossRef](#)]

30. Geoffrey, B.; David, L. Effect of annual signals on geodetic velocity. *J. Geophys. Res.* **2002**, *107*. [[CrossRef](#)]
31. Altamimi, Z.; Rebischung, P.; Métivier, L.; Collilieux, X. ITRF2014: A new release of the International Terrestrial Reference Frame modeling nonlinear station motions. *J. Geophys. Res. Solid Earth* **2016**. [[CrossRef](#)]
32. Dam, T.V.; Wahr, J.; Milly, P.C.D.; Shmakin, A.B.; Blewitt, G.; Lavallée, D.; Larson, K.M. Crustal displacements due to continental water loading. *Geophys. Res. Lett.* **2001**, *28*, 651–654.
33. King, M.A.; Watson, C.S.; Penna, N.T.; Clarke, P.J. Subdaily signals in GPS observations and their effect at semiannual and annual periods. *Geophys. Res. Lett.* **2008**, *35*, 247–255.
34. Penna, N.T.; Stewart, M.P. Aliased tidal signatures in continuous GPS height time series. *Geophys. Res. Lett.* **2003**, *30*, 69–73. [[CrossRef](#)]
35. Davis, J.L.; Wernicke, B.P.; Tamisiea, M.E. On seasonal signals in geodetic time series. *J. Geophys. Res. Atmos.* **2012**, *117*, 605–606. [[CrossRef](#)]
36. Bos, M.S.; Fernandes, R.M.S.; Williams, S.D.P.; Bastos, L. Fast error analysis of continuous GNSS observations with missing data. *J. Geod.* **2013**, *87*, 351–360. [[CrossRef](#)]
37. Williams, S.D.P. CATS: GPS coordinate time series analysis software. *GPS Solut.* **2008**, *12*, 147–153. [[CrossRef](#)]
38. Xu, C.; Yue, D. Characterizing noise in daily GPS position time series with overlapping Hadamard variance and maximum likelihood estimation. *Surv. Rev.* **2016**, *49*, 1–10. [[CrossRef](#)]
39. Le Bail, K. Estimating the noise in space-geodetic positioning: The case of DORIS. *J. Geod.* **2006**, *80*, 541–565. [[CrossRef](#)]
40. Collilieux, X.; van Dam, T.; Ray, J.; Coulot, D.; Métivier, L.; Altamimi, Z. Strategies to mitigate aliasing of loading signals while estimating GPS frame parameters. *J. Geod.* **2012**, *86*, 1–14. [[CrossRef](#)]
41. Klos, A.; Olivares, G.; Teferle, F.N.; Hunegnaw, A.; Bogusz, J. On the combined effect of periodic signals and colored noise on velocity uncertainties. *GPS Solut.* **2017**, *22*, 1. [[CrossRef](#)]
42. Plag, H.-P.; Pearlman, M. (Eds.) Global Geodetic Observing System. In *Meeting the Requirements of a Global Society on a Changing Planet in 2020*; Springer: Berlin/Heidelberg, Germany, 2009.
43. Blewitt, G. GPS Data Processing Methodology: From Theory to Applications. In *GPS for Geodesy*; Teunissen, P.G., Kleuberg, A., Eds.; Springer: Berlin, Germany, 1998; pp. 231–270.
44. Fritsche, M.; Sośnica, K.; Rodríguez-Solano, C.J.; Steigenberger, P.; Wang, K.; Dietrich, R.; Dach, R.; Hugentobler, U.; Rothacher, M. Homogeneous reprocessing of GPS, GLONASS and SLR observations. *J. Geod.* **2014**, *88*, 625–642. [[CrossRef](#)]
45. Lutz, S.; Meindl, M.; Steigenberger, P.; Beutler, G.; Sośnica, K.; Schaer, S.; Dach, R.; Arnold, D.; Thaller, D.; Jäggi, A. Impact of the arc length on GNSS analysis results. *J. Geod.* **2016**, *90*, 365–378. [[CrossRef](#)]



© 2018 by the authors. Licensee MDPI, Basel, Switzerland. This article is an open access article distributed under the terms and conditions of the Creative Commons Attribution (CC BY) license (<http://creativecommons.org/licenses/by/4.0/>).